Weierstraß-Institut
für Angewandte Analysis und Stochastik
Leibniz-Institut im Forschungsverbund Berlin e. V.

Preprint ISSN 2198-5855

Efficient current injection into single quantum dots through oxide-confined pn-diodes

Markus Kantner[1], Uwe Bandelow[1], Thomas Koprucki[1], Jan-Hindrik Schulze[2], André Strittmatter[2], Hans-Jürgen Wünsche[1,3,4]

submitted: October 22, 2015

[1] Weierstraß-Institut
Mohrenstr. 39
10117 Berlin
Germany
E-Mail: Markus.Kantner@wias-berlin.de
Uwe.Bandelow@wias-berlin.de
Thomas.Koprucki@wias-berlin.de
Hans-Juergen.Wuensche@wias-berlin.de

[2] Institut für Festkörperphysik
Technische Universität Berlin
Hardenbergstr. 36
10623 Berlin
Germany
E-Mail: j.schulze@tu-berlin.de
strittma@sol.physik.tu-berlin.de

[3] Ferdinand-Braun-Institut
Leibniz-Institut für Höchstfrequenztechnik
Gustav-Kirchhoff-Str. 4
12489 Berlin
Germany

[4] Humboldt Universität zu Berlin
Institut für Physik
Newtonstr. 15
12489 Berlin
Germany

No. 2169
Berlin 2015

2010 *Mathematics Subject Classification.* 65N08, 65Z05.

Key words and phrases. single-photon emitters, semiconductor device simulation, current confinement.

This work was supported by the German Research Foundation in the framework of the Collaborative Research Center SFB 787 *"Semiconductor Nanophotonics".*

Edited by
Weierstraß-Institut für Angewandte Analysis und Stochastik (WIAS)
Leibniz-Institut im Forschungsverbund Berlin e. V.
Mohrenstraße 39
10117 Berlin
Germany

Fax: +49 30 20372-303
E-Mail: preprint@wias-berlin.de
World Wide Web: http://www.wias-berlin.de/

Abstract

Current injection into single quantum dots embedded in vertical pn-diodes featuring oxide apertures is analyzed in the low-injection regime suitable for single-photon emitters. Experimental and theoretical evidence is found for a rapid lateral spreading of the carriers after passing the oxide aperture in the conventional pin-design. By an alternative design employing p-doping up to the oxide aperture the current spreading can be suppressed resulting in an enhanced current confinement and increased injection efficiencies, both, in the continuous wave and under pulsed excitation.

1 Introduction

Efficient electrical pumping of sub-micron sized domains is essential to achieve deterministic control over the carrier population within nanostructures such as quantum dots (QD). This is very important for the generation of single and entangled photons on-demand which is of high interest in the field of quantum optics, quantum information processing and quantum cryptography [1, 2]. Laterally oxidized apertures (OA) are widely implemented into GaAs/AlGaAs-based vertical cavity surface emitting lasers (VCSELs) to provide lateral current as well as optical confinement [3]. The insulating nature of the oxide leads to a funneling of charge carriers into the aperture within the oxide. Moreover, OAs modify the strain field and act as a stressor which has been successfully used to nucleate single QDs above such apertures deterministically [4, 5]. In combination with the current confinement supplied by the aperture a very efficient current injection scheme into single QDs can be expected. However, at low injection levels, our experimental and theoretical data reveal a minor effect of the aperture on the lateral current distribution. In a conventional pin-device layout, the carrier distribution laterally exceeds the dimension of the OA by several microns. Our analysis motivates a revised pn-junction design providing carrier confinement of the order of the aperture size at low injection levels. To fully understand the mechanisms that prevent efficient current funneling we simulated several alternative device designs with WIAS-TeSCA [6]. An improved design will be discussed in detail for both continuous wave (CW) and pulsed excitation.

2 Experimental

The basic design of a pn-diode featuring an OA is schematically shown in Fig. 1. By applying a two-step epitaxial process QDs can grow self-aligned at the mesa center due to the strain field of the OA. Using a procedure as detailed below, electrically driven single-photon sources (SPS) have been demonstrated recently. First, a 24-fold n-doped AlGaAs/GaAs distributed Bragg reflector (DBR) is grown followed by an AlAs/AlGaAs sandwich structure which later forms the OA. The DBR structure is intended to enhance the optical output through the surface of the device. Afterwards mesa structures are processed to expose the aperture layers and allow for wet chemical oxidation. Thereby an OA is formed acting as a buried stressor which laterally

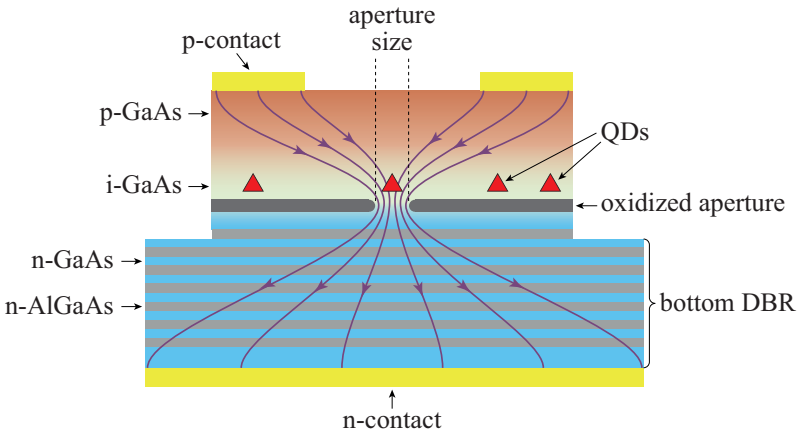

Figure 1: Schematic cross section of the device. The oxidized aperture controls the QD nucleation and the current confinement. The QD positions are indicated by triangles and the intuitive current flow is shown by purple lines.

modifies the strain field at the surface [7]. The QDs are subsequently grown as part of the second epitaxy in the Stranski-Krastanov (SK) growth mode. The growth ends with a p-doped contact layer. Formation of SK-QDs is strain driven where a 2D to 3D growth transition occurs at a certain critical layer thickness of about 1.7 mono-layers for $In_{0.65}Ga_{0.35}As$/GaAs [8]. Due to the lateral strain variation caused by the OA the QDs nucleate preferably at positions where the GaAs growth surface is tensilely strained. For small aperture diameters a single tensile strain maximum is formed directly above the aperture. Thus, it is possible to grow site-controlled QDs directly in the center of the mesa with a high selectivity to its surroundings [9]. Highly selective QD nucleation above the OA center is obtained for deposition amounts very close to the critical layer thickness for the 2D–3D transition. Fluctuations of the deposition amount across the lateral extension of the pn-junction region can hardly be avoided and therefore randomly occurring parasitic QD nucleation must be considered.

An electroluminescence map recorded at a lateral resolution of 1 µm of a 16 µm diameter pn-diode is shown in Fig. 2. Although this device does not show emission of a single central QD, it was chosen to demonstrate the insufficient current confinement by the oxide aperture. Within a range of 10–600 nA current injection excitation of several randomly nucleated parasitic QDs is revealed. While the aperture diameter of this particular device is around 800 nm, even QDs located about 7 µm away from the mesa center can be electrically excited. This observation is a contradiction to the naive expectation of the current paths as indicated in Fig. 1. Apparently, the current confinement due to the OA is weak. From the scaling of the device resistance with the diameter of the OA an insulating property of the oxide is concluded. Consequently, a rapid lateral current spreading after the aperture causing parasitic QD excitation has to be considered.

We use numerical simulations of the charge carrier transport to understand the lateral current spreading after the OA in detail. The simulations are particularly aimed at low injection currents and cryogenic temperatures as the typical operation conditions of electrically driven SPS.

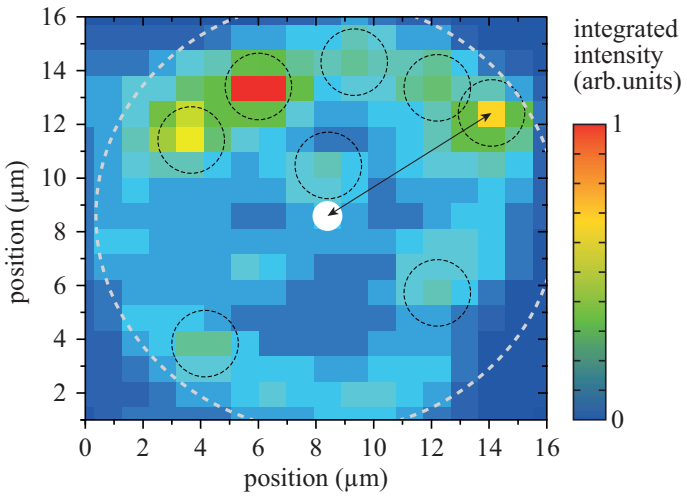

Figure 2: Electroluminescence map of a mesa at 10 nA with several parasitic QDs. White circle denotes the OA. The arrow corresponds to a distance of 6.7 µm between a parasitic QD and the OA.

3 The model of current flow

The excitation of QDs across the whole mesa region is counterintuitive since the radius of the mesa is much larger than the aperture radius and also exceeds typical charge carrier diffusion lengths. Consequently, the carriers injected through the aperture should not be able to reach the parasitic QDs. The experimental finding described above contradicts this expectation.

In order to fully understand this phenomenon, we have studied the current spreading with the simulation tool WIAS-TeSCA [6]. It solves the van Roosbroeck system of equations [10], which is a coupled system of the nonlinear Poisson's equation

$$-\nabla \cdot \varepsilon_0 \varepsilon_r \nabla \psi = e\left(p - n + N_D^+ - N_A^-\right) \tag{1}$$

and a continuity equation for each carrier species

$$\begin{aligned} e\frac{\partial p}{\partial t} + \nabla \cdot \mathbf{j}_p &= -eR, \\ -e\frac{\partial n}{\partial t} + \nabla \cdot \mathbf{j}_n &= +eR. \end{aligned} \tag{2}$$

Here ψ is the electrostatic potential, n and p denote the electron and hole density, respectively, e is the elementary charge, ε_r is the dielectric constant of the semiconductor, ε_0 is the vacuum permittivity, and R combines various recombination mechanisms (Shockley-Read-Hall recombination, Auger recombination, radiative recombination). The ionized donor and acceptor densities are labeled by N_D^+ and N_A^-. The current densities $\mathbf{j}_n$ and $\mathbf{j}_p$ are modeled in a standard way as drift and diffusion currents [11]. Details and parameters are given in the appendix.

Two cylindrical mesa designs are compared, which differ only in their doping profile (Fig. 3). The pin-design with layer thickness and doping parameters close to the experimental structure is investigated first. The intrinsic layer will be denoted by *cavity* (even though it is not an optical

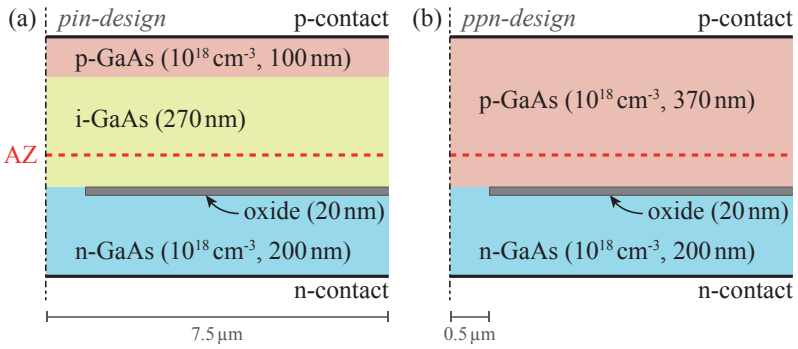

Figure 3: Sketches of the essential cross sections of the two simulated axisymmetric device structures. The pin-design (a) contains a 270 nm thick intrinsic layer between the n- and p-doped regions. In the ppn-design (b), this layer is also p-doped. The dashed red line labeled AZ is the position of the QD layer. The QDs are disregarded in the macroscopic transport calculations (see text). The thickness of the current-blocking oxide on top of the n-layer is set to 20 nm. The diameter of the aperture in the center is 1 µm. Except for the oxide, the material is throughout GaAs.

cavity) and the embedded QD layer located 135 nm above the oxide is called *active zone* (AZ). Some details of the experimental structure (cf. Fig. 1) have marginal influence on the current distribution between aperture and AZ and are therefore simplified in the model. The highly conducting cap layer is modeled just as an ohmic contact, neglecting the minimal potential drop across the layer. The same is done to model the complete bottom DBR. Thereby, the interesting current flow between aperture and AZ is decoupled from the complex phenomena in the top and bottom layers of the device. For the same reason, the detailed multi-layer aperture region of real devices is reduced to a single current-blocking insulator in GaAs with a hole diameter of 1 µm and a thickness of 20 nm. In the simulations, the device temperature is set to $T = 30\,\mathrm{K}$ throughout the paper. It is worth to note here, that device simulation at cryogenic temperatures is challenging for the modeling, as well as for the numerics [12], as will be pointed out in the appendix.

It is generally difficult to model the AZ as an ensemble of QDs. This layer is on average only 2.2 mono-layers thick, has at least a corrugated surface if not a pure 3D discontinuous structure and the QDs are randomly distributed. Obviously, the consideration of one particular realization of such a layer is without any meaning. Fortunately, the recombination lifetimes in the QDs and the surrounding GaAs are roughly equal. Under these conditions, the impact of the particular random realization of the AZ on the macroscopic current distribution is marginal and can be neglected. With this in mind, the random InGaAs layer is replaced by a homogeneous GaAs-AZ of constant thickness in the simulations.

In the following, we analyze CW operation of this structure and give an explanation for the excitation of the parasitic QDs. Moreover, we demonstrate appropriate current funneling in an alternative pnn-design, which is then also analyzed in the case of pulsed operation.

4 Analysis of low injection CW operation in the pin-design

Under CW operation, the carrier density in the AZ increases rapidly with the bias voltage U, in particular in the cryogenic situation. This is shown in Fig. 4 (a). Also the radial distribution changes when moving from the low-injection to the high-injection case. The density is nearly constant in case of low-injection and starts to drop outwards for higher injections.

To quantify the suitable injection regime for single-photon emission we avoid the cumbersome quantum theory of the coupled QD-photon system, since the following simple consideration gives an sufficient estimate for the intended purpose. Emission of indistinguishable photons is achieved if perturbation of the quantum system by other charge carriers is suppressed during the emission process. As a basic requirement charge carrier capture times τ_c longer than the lifetime τ of the quantum state must be realized. Otherwise further capture events can change the initial state before or "during" the emission. The upper boundary for the capture time results from the target of high single-photon emission rates which means immediate supply of charge carriers to the QD after each emission event. Hence, the optimal regime for single-photon emission is $\tau_c \approx \tau \approx 1\,\text{ns}$. The capture rate is roughly proportional to the bulk carrier density n in the vicinity of the QD [13, 14], i.e.

$$\tau_c^{-1} = \kappa n \qquad \text{with} \qquad \kappa \approx 10^{-6}\,\text{cm}^3\text{s}^{-1},$$

corresponding to a typical capture time of 1 ps at a density of $10^{18}\,\text{cm}^{-3}$. Capture times of this order of magnitude have been reported for rather different QD embeddings, see e.g. [14, 15]. Thus, optimum single-photon emission requires densities of the order of $10^{15}\,\text{cm}^{-3}$. Henceforth we focus our analysis to this density range, which belongs to the low injection regime.

In this regime, the density in Fig. 4 (a) is roughly independent of the radial position in the AZ. Since the capture rate is assumed to be proportional to the density, filling of a QD is expected to be independent on the radial position. This assumption agrees well with the large excitation probability of parasitic QDs described in Sec. 2.

The internal physics behind is also illustrated in Fig. 4. The electrons flow around the aperture (Fig. 4 (b)) and outwards in a thin layer on top of the oxide, where the electron density reaches nearly $10^{18}\,\text{cm}^{-3}$ (dark red in Fig. 4 (c)). This well-conducting layer is radially homogeneous and acts like an equipotential plane. As a consequence, the electron distribution everywhere above it and, in particular, the injection into the AZ becomes also almost homogeneous along the radial direction.

At first glance, the high electron mobility might be responsible for the electrons to spread so rapidly. Therefore, it should be beneficial to inject holes through the aperture, whose mobility is much smaller. We accounted for this consideration by exchanging n and p doping, but simulations of a corresponding nip-design yielded nearly no improvement. The holes spread radially along the mesa as well, irrespective of their short diffusion length. We concluded the mobility is secondary for the extreme spreading in the low-injection regime. Returning to the analysis of the pin-sample, we found a more important factor of influence. Within the intrinsic layer above the oxide, the density of the holes is orders of magnitude smaller than the electron density. This fact renders that the recombination rate R becomes extremely small. At low temperatures and when other recombination pathways are not limiting, the electron life time $\tau_n = n/R$ becomes

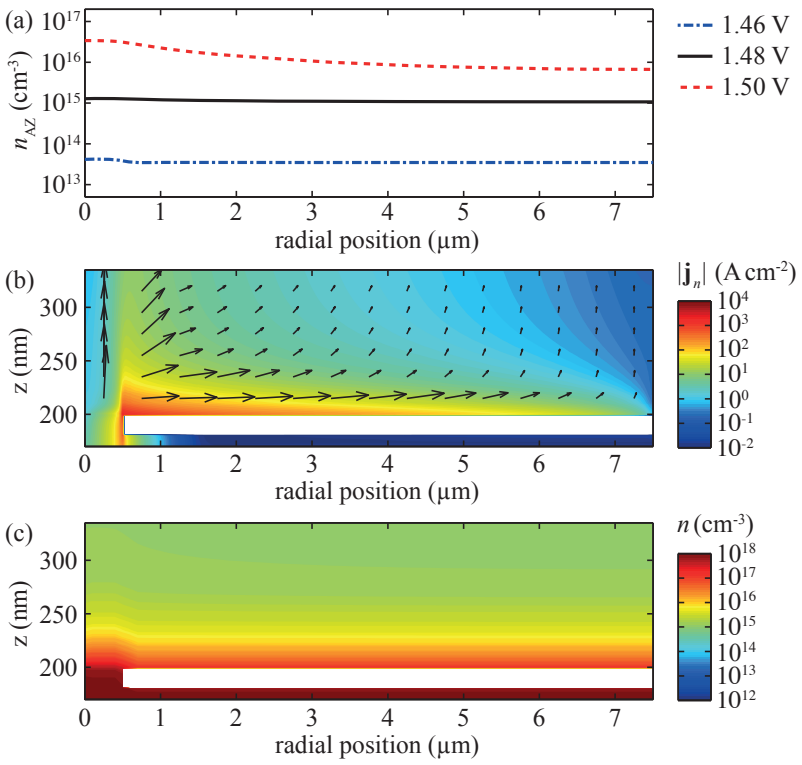

Figure 4: Analysis of the pin-design. (a) Radial profile of the carrier distributions within the AZ for selected CW bias voltages. Electron and hole densities are identical since the AZ lies in the middle of the intrinsic layer. (b) Electron flow (arrows) and magnitude (color coded) between oxide (white) and AZ (top border) at $U = 1.48$ V. (c) Electron density in the same cross section.

necessarily extremely long. The simulations yield τ_n up to milliseconds. With such lifetimes, the diffusion length exceeds the mesa radius by orders of magnitude and the electrons can easily fill the whole mesa area.

Motivated by the importance of this situation, we stress that it is not the matter of the corresponding specific doping configuration, but a general feature of any design containing an intrinsic layer of sufficient thickness under low injection. The space charge zone extends over nearly the whole intrinsic layer. Close to its n-side, it holds $p \ll n$. Furthermore, the Shockley-Read-Hall recombination is dominant and an elementary calculation yields the effective lifetimes

$$\tau_p = \tau_{p0} \quad \text{and} \quad \tau_n = \frac{n}{p}\tau_{p0} \gg \tau_p.$$

Mutatis mutandis for the p-side border of the intrinsic layer. The lifetime of the majority exceeds that of the minority by several orders of magnitude. The unwanted giant excitation spreading in the low-injection regime is an unavoidable consequence of the cavity being undoped. On the other hand, for devices like LEDs and VCSELs operating under high-injection where diffusion is dominant, the effect of lateral current spreading is minor.

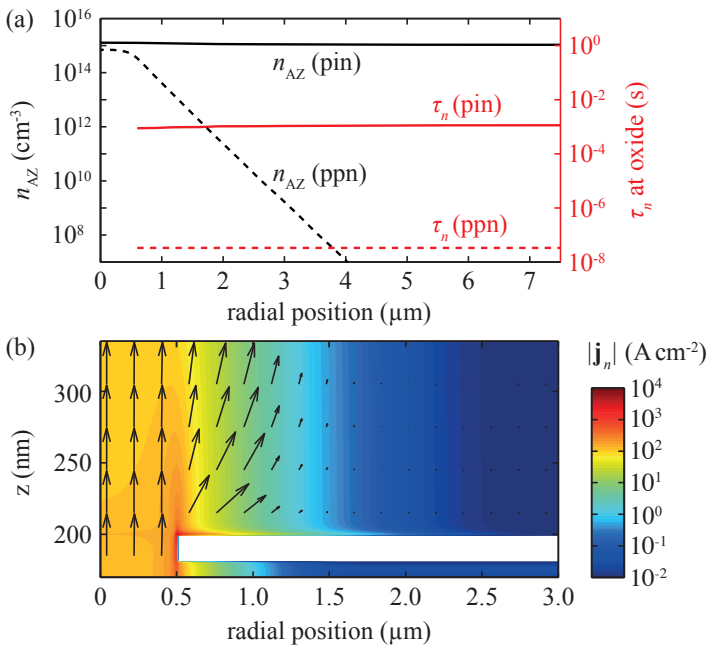

Figure 5: (a) Radial distributions of the electron density $n_{\mathrm{AZ}}(r)$ in the AZ (black) and the electron life time τ_n just above the oxide (red). Solid lines are for the pin-design, dashed lines for the ppn-design where the cavity is p-doped with $N_A = 10^{18}\,\mathrm{cm}^{-3}$. The maximal electron density in the AZ is near $n_{\mathrm{AZ}}(0) = 10^{15}\,\mathrm{cm}^{-3}$ in both cases. (b) Electron current density distribution in the central region between oxide (white) and the AZ (top border) in the ppn-design. Arrows indicate the direction of electron flow, the magnitude is color coded. Note the different radial scale compared to Fig. 4.

5 CW current confinement in a ppn-design

Considering the findings of Sec. 4, doping of the cavity region will likely be helpful to suppress the current spreading. The simulation results presented in Fig. 5 for a corresponding ppn-design confirm this expectation. The electron lifetime becomes small (Fig. 5 (a)) and the current spreading is drastically reduced (Fig. 5 (b)). Accordingly, the radial electron concentration in the AZ decreases rapidly with r, suppressing the excitation of parasitic QDs, see Fig. 5 (a).

Due to the p-doping above the oxide, the injected electrons become minorities and the electron flow is dominated by diffusion. Interestingly, the diffusion length corresponding to the reduced lifetime is still much larger than the radial decrease of $n_{\mathrm{AZ}}(r)$. The additional confinement is related to the vicinity of the p-contact. A considerable part of the injected electrons recombines at the contact, further reducing the mean lifetime. The contact induced lifetime can be estimated as $\tau_c \approx d^2/2D$, where d is the distance between oxide and contact and $D = k_B T \mu / e$ is the diffusion coefficient. Our parameters yield $\tau_c \approx 40\,\mathrm{ps}$, which is nearly three orders of magnitude below the bulk τ_n in Fig. 5 (a) and explains the steep decrease of $n_{\mathrm{AZ}}(r)$.

Concluding so far, the radially homogeneous excitation of the AZ across the whole mesa area is the consequence of keeping the cavity undoped in the standard pin-design. In contrast, the current can be funneled much more to the central QD by using a ppn-design with sufficient

cavity doping, e.g. $N_A \approx 10^{18}\,\mathrm{cm}^{-3}$ in combination with a small total thickness of the p-layers. The total current increases by these measures. This increase has to be paid to compensate for the larger total recombination. In our simulations, the current for achieving $n_{\mathrm{AZ}} = 10^{15}\,\mathrm{cm}^{-3}$ doubles approximately. This factor is not much in light of the excellent current funneling in a SPS. As a further consequence of doping the AZ, the emission properties of the QDs will be altered. Due to the p-doping, emission of positively charged complexes (e.g. trions) will become more likely. In turn, this will decrease the emission from the neutral exciton and bi-exciton. Trion emission exhibits no fine structure splitting which is advantageous for single-photon generation.

6 Pulsed operation

For practical applications of a SPS the deterministic triggering of each photon emission event is essential [2]. Hence, a SPS will be operated in pulsed excitation mode. Furthermore, high repetition rates of the order of GHz are desirable. This requires accordingly short pump pulses. In this section we investigate whether the results of current spreading under CW excitation hold for the dynamic case of pulsed operation.

To answer this question, we apply 100 ps long bias pulses with a repetition rate of 1 GHz on top of a constant bias voltage U_0. The bias voltage is chosen just below the threshold voltage of the pn-diode, such that the electron density in the AZ is slightly below $10^{12}\,\mathrm{cm}^{-3}$. Under these conditions the capture time of the QD is beyond 1 µs, which suppresses captures between pulses. The pulse height ΔU is chosen such that the capture time raises to the order of the pulse length. The rise and fall time is 20 ps each.

The evolution of the radial electron distributions is illustrated in Fig. 6. The responses of both designs follow the bias pulse with a delay of only a few picoseconds. We conclude, the internal electronic processes in the cavity are sufficiently fast for pulsed single-photon emission with high repetition rates. Limitations will come from external effects like parasitic capacitances and inductivity of bond wires. These items are not subject of present paper.

The radial distribution $n_{\mathrm{AZ}}(r,t)$ differs drastically between the two designs under pulsed operation. In the pin-design, it rises homogeneously until about $10^{15}\,\mathrm{cm}^{-3}$ is reached. Thereafter, the rise is stopped above the oxide. But it continues to about $10^{16}\,\mathrm{cm}^{-3}$ above the aperture. Accordingly, the probability to capture an electron during the pulse is about 100 % for the central QD but only about 10 % in the outer region of the mesa. This represents a noticeable reduction of the capture rate for parasitic QDs compared to CW operation but it is probably not small enough to ensure pure single-photon emission of the device. The pulse-response of the ppn-design is entirely restricted to the central part of the mesa. The diameter of the excitation area, where the capture probability of a QD exceeds 1 %, is only about 3 µm. Thus, both under CW and pulsed operation, the ppn-design is distinctly better suited for current funneling towards the central QD than the pin-design.

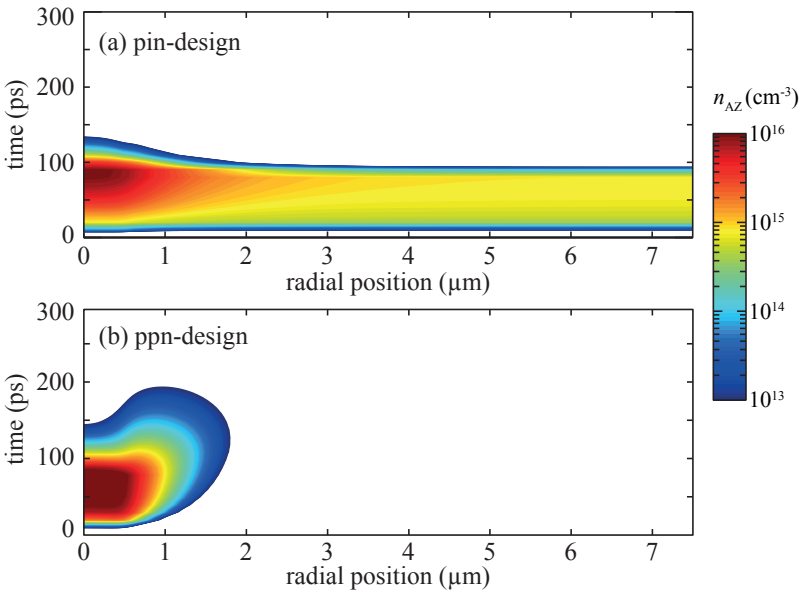

Figure 6: Response of the electron density in the AZ to a periodically pulsed contact voltage (see text for details). (a) pin-design ($U_0 = 1.43$ V, $\Delta U = 70$ mV), (b) ppn-design ($U_0 = 1.48$ V, $\Delta U = 30$ mV). Time is measured relative to the onset of the respective bias pulse. White areas indicate very small electron densities lower than 10^{13} cm^{-3}.

7 Conclusion

We have shown that the current confinement by a small aperture in an oxide layer can fail under low current injection as applied for single-photon generation with QD-based SPS. The unintended current spreading is caused by huge differences of the minority and majority charge carrier lifetimes for the given operating conditions. These differences are a direct consequence of the intrinsic region in an pin-design. Our simulations have shown that doping of the active region leads to much greater current confinement both for CW and pulsed operation. Under pulsed operation the lateral current spreading can be reduced down to a diameter of 3 µm for an 1 µm wide aperture.

Appendix: Model equations and parameters

The fundamental Poisson- and continuity equations (1) and (2) are supplemented by the following model assumptions for GaAs at $T = 30$ K. The relative dielectric constant is taken as $\varepsilon_r = 12.9$ [16] and the recombination rate is

$$R = \left(np - n_i^2\right)\left(\frac{1}{n\tau_{p0} + p\tau_{n0}} + B + C_n n + C_p p\right)$$

with $\tau_{p0} = 34\,\text{ns}$, $\tau_{n0} = 10\,\text{ns}$, $B = 10^{-8}\,\text{cm}^3\,\text{s}^{-1}$, and $C_n = C_p = 10^{-30}\,\text{cm}^6\,\text{s}^{-1}$. The current densities, carrier densities and the electrostatic potential are related by

$$\begin{aligned} \mathbf{j}_n &= \mu_n n \nabla F_n, \quad n = N_c \mathcal{F}\left(\tfrac{F_n - E_c + e\psi}{k_B T}\right) \\ \mathbf{j}_p &= \mu_p p \nabla F_p, \quad p = N_v \mathcal{F}\left(\tfrac{E_v - e\psi - F_p}{k_B T}\right) \end{aligned} \tag{3}$$

with the Fermi-Dirac integral of order 1/2

$$\mathcal{F}(\eta) = \frac{2}{\sqrt{\pi}} \int_0^\infty \mathrm{d}y \, \frac{\sqrt{y}}{\exp(y - \eta) + 1}.$$

The charge carrier mobilities are assumed as $(\mu_n, \mu_p) = (10^4, 300)\,\text{cm}^2\,\text{V}^{-1}\,\text{s}^{-1}$ and $(\mu_n, \mu_p) = (6400, 130)\,\text{cm}^2\,\text{V}^{-1}\,\text{s}^{-1}$ in the intrinsic and doped material, respectively [17]. The effective band densities at $T = 30\,\text{K}$ are $(N_c, N_v) = (1.25, 30) \times 10^{16}\,\text{cm}^{-3}$ and the band gap is $E_c - E_v = 1.5\,\text{eV}$. The Fermi levels (F_n, F_p) are calculated from Eqs. (1) and (2) after inserting (3).

The boundary conditions at the Ohmic contacts are $F_n = F_p = eU_i$ and local charge neutrality, where U_i denotes the external voltage applied to contact i. At the other boundaries, the normal components of $\nabla\psi$, $\mathbf{j}_n$ and $\mathbf{j}_p$ vanish.

In the supposed cryogenic situation the thermal energy is approximately ten times smaller than at room temperature. The carrier densities scale exponentially with the inverse thermal energy as in Eq. (3). Consequently small differences between the band edge energy and the carriers quasi Fermi energy are exponentially enhanced and result in domains with either a very low (depleted semiconductor) or very high (degenerate semiconductor) carrier density, separated by very narrow boundary layers in the thermal equilibrium. In this case the carrier densities need to be described by the Fermi-Dirac distribution, the Boltzmann approximation is not valid anymore at cryogenic temperatures. For built-in dopant densities below the critical density of the metal-insulator transition [18] one has to take incomplete ionization effects into account. However, for p-doped GaAs:C the critical acceptor density is given by $N_A^{\text{crit}} \approx 10^{18}\,\text{cm}^{-3}$ [19] and therefore we assume $N_A^- \approx N_A$ throughout the paper.

References

[1] C. Santori, D. Fattal, and Y. Yamamoto, *Single-photon Devices and Applications*. Weinheim: Wiley-VCH, 2010.

[2] S. Buckley, K. Rivoire, and J. Vučković, "Engineered quantum dot single-photon sources," *Rep. Prog. Phys.*, vol. 75, no. 12, p. 126503, Nov 2012.

[3] R. Michalzik, Ed., *VCSELs – Fundamentals, Technology and Applications of Vertical-Cavity Surface-Emitting Lasers*, Springer Series in Optical Sciences. Berlin, Heidelberg: Springer, 2013.

[4] W. Unrau, D. Quandt, J.-H. Schulze, T. Heindel, T. D. Germann, O. Hitzemann, A. Strittmatter, S. Reitzenstein, U. W. Pohl, and D. Bimberg, "Electrically driven single photon source based on a site-controlled quantum dot with self-aligned current injection," *Appl. Phys. Lett.*, vol. 101, no. 21, p. 211119, 2012.

[5] A. Strittmatter, A. Holzbecher, A. Schliwa, J.-H. Schulze, D. Quandt, T. D. Germann, A. Dreismann, O. Hitzemann, E. Stock, I. A. Ostapenko, S. Rodt, W. Unrau, U. W. Pohl, A. Hoffmann, D. Bimberg, and V. Haisler, "Site-controlled quantum dot growth on buried oxide stressor layers," *Phys. Status Solidi A*, vol. 209, no. 12, pp. 2411–2420, Nov 2012.

[6] WIAS-TeSCA. http://www.wias-berlin.de/software/tesca/

[7] F. Kießling, T. Niermann, M. Lehmann, J.-H. Schulze, A. Strittmatter, A. Schliwa, and U. W. Pohl, "Strain field of a buried oxide aperture," *Phys. Rev. B*, vol. 91, no. 7, Feb 2015.

[8] F. Heinrichsdorff, "MOCVD growth and laser applications of In(Ga)As/GaAs quantum dots," Ph.D. dissertation, Technical University of Berlin, 1998.

[9] A. Strittmatter, A. Schliwa, J.-H. Schulze, T. D. Germann, A. Dreismann, O. Hitzemann, E. Stock, I. A. Ostapenko, S. Rodt, W. Unrau, and et al., "Lateral positioning of InGaAs quantum dots using a buried stressor," *Appl. Phys. Lett.*, vol. 100, no. 9, p. 093111, 2012.

[10] W. van Roosbroeck, "Theory of the flow of electrons and holes in germanium and other semiconductors," *Bell Sys. Tech. J.*, vol. 29, no. 4, pp. 560–607, Oct 1950.

[11] S. L. Chuang, *Physics of Photonic Devices*. Hoboken, New Jersey: Wiley, 2009.

[12] M. Kantner, U. Bandelow, T. Koprucki, and H.-J. Wünsche, "Modeling and numerical simulation of electrically pumped single-photon emitters," in *Proceedings of the 15th International Conference on Numerical Simulation of Optoelectronic Devices 2015*, J. Piprek and Y.-R. Wu, Eds., Taipei, Taiwan, September 2015, pp. 151–152.

[13] A. Wilms, "Coulomb induced interplay of localized and reservoir carriers in semiconductor quantum dots," Ph.D. dissertation, Technical University of Berlin, 2013.

[14] A. Wilms, P. Mathé, F. Schulze, T. Koprucki, A. Knorr, and U. Bandelow, "Influence of the carrier reservoir dimensionality on electron-electron scattering in quantum dot materials," *Phys. Rev. B*, vol. 88, no. 23, Dec 2013.

[15] T. Switaiski, U. Woggon, D. E. Alden Angeles, A. Hoffmann, J.-H. Schulze, T. D. Germann, A. Strittmatter, and U. W. Pohl, "Carrier dynamics in InAs/GaAs submonolayer stacks coupled to Stranski-Krastanov quantum dots," *Phys. Rev. B*, vol. 88, no. 3, Jul 2013.

[16] M. Levinstein, S. Rumyantsev, and M. Shur, *Handbook Series on Semiconductor Parameters vol. 2*. Singapore, New Jersey, London, Hongkong: World Scientific, 1996.

[17] V. Palankovski and R. Quay, *Analysis and Simulation of Heterostructure Devices*, Series on Computational Microelectronics. Vienna: Springer Science & Business Media, 2004.

[18] N. F. Mott, "Metal-Insulator Transition," *Rev. Mod. Phys.*, vol. 40, no. 4, pp. 677–683, Oct 1968.

[19] A. Ferreira da Silva, "Electrical resistivity of acceptor carbon in GaAs," *J. Appl. Phys.*, vol. 95, no. 5, p. 2532, 2004.